TU Delft

Delft University of Technology

Predicting the response of complex systems for coastal management

Hendrickx, Gijs G.; Antolínez, José A.A.; Herman, Peter M.J.

DOI
10.1016/j.coastaleng.2023.104289

Publication date
2023

Document Version
Final published version

Published in
Coastal Engineering

Citation (APA)
Hendrickx, G. G., Antolínez, J. A. A., & Herman, P. M. J. (2023). Predicting the response of complex systems for coastal management. *Coastal Engineering*, *182*, Article 104289. https://doi.org/10.1016/j.coastaleng.2023.104289

Important note
To cite this publication, please use the final published version (if applicable).
Please check the document version above.

Copyright
Other than for strictly personal use, it is not permitted to download, forward or distribute the text or part of it, without the consent of the author(s) and/or copyright holder(s), unless the work is under an open content license such as Creative Commons.

Takedown policy
Please contact us and provide details if you believe this document breaches copyrights.
We will remove access to the work immediately and investigate your claim.

This work is downloaded from Delft University of Technology.
For technical reasons the number of authors shown on this cover page is limited to a maximum of 10.

Coastal Engineering 182 (2023) 104289

Contents lists available at ScienceDirect

Coastal Engineering

journal homepage: www.elsevier.com/locate/coastaleng

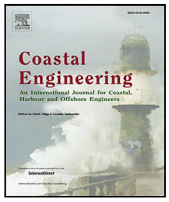

Predicting the response of complex systems for coastal management

Gijs G. Hendrickx [a,*], José A.A. Antolínez [a], Peter M.J. Herman [a,b]

[a] Department of Hydraulic Engineering, Delft University of Technology, Delft, The Netherlands
[b] Unit Marine and Coastal Systems, Deltares, Delft, The Netherlands

ARTICLE INFO

Keywords:
Adaptive sampling
Building with Nature
Estuary
Hybrid modelling
Machine learning
Risk management

ABSTRACT

In recent years, coastal management has been facing new challenges: socio-economic growth and consequent climate change impose new boundary conditions pushing coastal systems towards unseen states. For adaptation and mitigation strategies as well as risk management, the resilience of systems to these projected changes must be tested and quantified using predictive tools, given the scarcity of observations. Process-based models, which limit the number of assumptions, are the preferred tools. However, these models are computationally expensive and therefore unattractive for global sensitivity and uncertainty analyses. Input and model reduction techniques, as well as behavioural empirical models, have been widely used to overcome these computational difficulties. In this paper, we propose a process-based hybrid workflow—that combines statistical and machine learning with a process-based numerical model—to provide sensitivity analyses on complex systems. As an example we explore salt intrusion in estuaries. The novelty of the method presented is the implementation of an adaptive sampling technique of numerical experiments with a process-based hydrodynamic model, and the training of a neural network to augment the set of numerical runs executed. The first uses predictive uncertainty to automatically explore the response of the complex system to varying environmental boundary conditions and geomorphological configurations. The second is trained to provide system responses around the sampled points. This exploration is closed by simulating the extremes in the output space as found by a genetic algorithm. This scheme is shown to be highly efficient in non-linear, heteroscedastic, and highly non-stationary systems.

1. Introduction

In recent years, the effects of climate change have become more apparent (e.g. Harley et al., 2006; Veldkamp et al., 2015; Vörösmarty et al., 2000; Walther et al., 2002) and with it the need for preparing for the unknown: Natural systems venture out to extremes often absent from the records. Examples of such extremes include the recent droughts in northwestern Europe caused by an extremely low river discharge in the Rhine (Toreti et al., 2022); the increased frequency of mass coral bleaching events recorded over the past decades (Hughes et al., 2018); and the so-called *Black Summer* of 2019/2020 during which an exceptionally large area of Australia's southeast coast was consumed by wildfires (Collins et al., 2021). In addition, sea level rise shifts whole coastlines to new territories and possible modified system responses, as new areas might get inundated.

These changing conditions challenge risk management practices (van Berchum et al., 2019) and require the revision of adaptation and mitigation strategies (Haasnoot et al., 2014). Therefore, explorations to map the impacts of these changing conditions on current land-use as well as determining future-proof socio-ecological systems are necessary. Key in such studies is to achieve a system understanding. While surveying and monitoring often provide insightful knowledge, in this phase, numerical models are a necessity to predict system responses to unseen forcing, socio-economic boundary conditions, and/or human interventions.

This system understanding can be achieved by means of a sensitivity analysis of the system's response to changing conditions; this may include the boundary conditions as well as the geomorphological characteristics. In addition, a proper parameterisation of the physical system and processes in the numerical model is key and non-trivial. Consequently, sensitivity analyses often require experimental designs that rely on a large number of samples. Examples are those following factorial sampling (e.g. Wang et al., 2020) or Monte Carlo sampling (e.g. Saltelli et al., 1999; Saltelli, 2002).

In practice, large experimental designs could be accomplished by running a large number of numerical simulations, often impractical if they were set-up with complex, and thus computationally expensive, hydraulic engineering numerical models, e.g. Delft3D Flexible Mesh (DFM; Deltares, 2022) or Finite-Volume Community Ocean

* Corresponding author.
E-mail address: G.G.Hendrickx@tudelft.nl (G.G. Hendrickx).

https://doi.org/10.1016/j.coastaleng.2023.104289
Received 22 November 2022; Received in revised form 27 January 2023; Accepted 17 February 2023
Available online 1 March 2023
0378-3839/© 2023 The Author(s). Published by Elsevier B.V. This is an open access article under the CC BY license (http://creativecommons.org/licenses/by/4.0/).

Model (FVCOM; Chen et al., 2013). Therefore, executing such analyses would result in a computationally infeasible task (Saltelli, 2002).

Traditionally, hydraulic engineers have addressed this problem by (1) developing a series of model reduction techniques; and (2) acceleration of the direct simulations. Regarding model reduction techniques, common practices are:

1. the use of statistical downscaling, for example, to develop parameterisations of physical processes (e.g. Bruun, 1954; Stockdon et al., 2006), or to infer the response of coastal systems to larger scale forcing (e.g. Anderson et al., 2018; Antolínez et al., 2018);
2. the development of behavioural models that combine multiple of these physics-driven statistics using basic knowledge principles, for example shoreline models (e.g. Antolínez et al., 2019; Ashton et al., 2001; Kragtwijk et al., 2004); and
3. the simplification of numerical models by neglecting certain physical processes in favour of faster running times of which the hydrostatic assumption is the most broadly used in hydrodynamic models (default settings in, e.g., DFM and FVCOM; Deltares, 2022; Chen et al., 2013, resp.).

Regarding the acceleration of the direct simulations, these are often achieved by: (1) developing acceleration techniques (de Vriend et al., 1993; Luijendijk et al., 2019), and (2) using input reduction techniques (Antolínez et al., 2016; Hendrickx et al., 2021; Latteux, 1995; Walstra et al., 2013).

In addition to these reduction techniques, the use computationally expensive models generally rely on expert judgement to decide the limited number of simulated samples (e.g. Ralston et al., 2010; Warner et al., 2005); the most efficient reduction technique remains limiting the number of simulations. However, sampling based on expert judgement limits the investigation to the expected: exploring unknown territories is computationally too expensive and therefore discouraged. On the other hand, simplified models limit the output to the assumptions made due to the simplifications (e.g. Kuijper and van Rijn, 2011; MacCready, 1999), which might result in essential processes to be overlooked. Ideally, process-based models can be used for exploratory research of complex systems without skyrocketing computational costs.

Currently, hybrid experimental designs are being adopted to perform larger numbers of simulations (e.g. Camus et al., 2011; Bakker et al., 2022). This so-called Hybrid Downscaling (HD) often contains the following three phases: (1) the sampling of representative input or boundary conditions (Athanasiou et al., 2021; Scott et al., 2020); (2) the simulation of these samples in a numerical model; and (3) the augmentation of the modelled output for the whole input space, which is either achieved statistically (e.g. Rueda et al., 2019; Scott et al., 2020) or using machine learning techniques (e.g. Athanasiou et al., 2022; Itzkin et al., 2022).

Most of the selection schemes deployed in HD select samples in an input space without knowing information about the (often non-linear) response of the system (e.g. Latin hypercube sampling [McKay et al., 1992]; maximum dissimilarity algorithm [Kennard and Stone, 1969]; self-organising maps [Kohonen, 1982]). This turns into an inefficient and costly exploration (e.g. Gramacy and Lee, 2009; Ruessink, 2006). The efficiency of the exploration is expected to improve substantially when the input space considers the available information about the output space when sampling (Gramacy and Lee, 2009). Hence, to influence the selection of samples in the input space by a reduced number of model simulations, a two-step approach is required in which the input space is adaptively updated based on the known part of the output space.

In this paper, we develop such an adaptive sampling scheme tailored to hydraulic engineering models, such as the aforementioned hydrodynamic models DFM and FV-COM. In this scheme, the sampling in the input space is influenced by the system's response at the previous selected representative samples, requiring to run the model sequentially in parallel batches, promoting a more efficient exploration.

The second phase—the numerical modelling—is executed with a process-based model: DFM (Deltares, 2022). This ensures that the bias of known fitted parameters is limited when exploring unknown regions in the input space.

The last phase in HD—the augmentation—has received substantial attention over the years. Augmentation methods range from very simplistic procedures such as look-up tables or linear interpolation to more complex regression methods based on statistical and/or probabilistic models. In addition, machine learning is currently gaining popularity and has shown great potential in many fields of research, as in machine learning probability and statistics can coexist. This rise has led to opt for the inclusion of both generative and discriminative machine learning models (Jebara, 2004), such as a treed Gaussian process, limiting linear model (TGP-LLM; Gramacy and Lee, 2009) and a neural network, respectively.

Hence, the overall aim of this paper is to provide a methodology for gaining as much information about a complex system for the lowest computational costs. This is applied on a case study implementing the *Building with Nature*-approach. In the application, we address the question how machine learning techniques can assist in applying the *Building with Nature*-approach, i.e. developing nature-based solutions. A sensitivity analysis is at the basis of understanding the system and machine learning tools are implemented to assist in this goal.

To answer the research question, this paper starts with a description of the proposed methodology (Section 2) after which it is applied on a case study introduced in Section 3: salt intrusion in estuaries. Subsequently, the implications of this newly proposed work-flow are presented and discussed in which the required sample size—or stopping rule—receives additional attention (Sections 4 and 5, resp.). At last, the pros and cons of the simulations strategy are summarised in Section 6.

2. Method

The many available techniques introduced in Section 1 have been evaluated and distilled down to a five-step simulation strategy (Fig. 1): (1) generate candidate samples, (2) simulate an initial batch, (3) execute an adaptive sampling approach, (4) simulate reverse-predicted extremes, and (5) augment the input space. These five steps are also visualised in Fig. 1, stating the sample sizes as used in this study. Every step and the sampling techniques used are further elaborated on in Sections 2.1–2.5.

2.1. Candidate samples

The first step is to create a data set with candidate samples. These candidate samples were based on predefined parameter ranges, which reflected physically representative values. When generating the candidate samples, it is important to include a physical check of the samples: although the parameter ranges make physically sense, certain combinations may not. For example, a realistic river discharge of 16000 m^3s^{-1} and a realistic cross-sectional area of 2500 m^2 result in an unrealistically high river flow velocity of 6.4 ms^{-1}. By applying physical checks—and subsequently using the resulting candidate samples—the physical correctness of the parametric design is enforced.

2.2. Initial batch

The second step is to create—and simulate—an initial batch to initiate the subsequent adaptive sampling routine. In this study, the Maximum Dissimilarity Algorithm (MDA; Kennard and Stone, 1969) was used to do so, as it best explores the outskirts of the input space by choosing the most dissimilar samples from the candidate samples. At this stage, little is known about the response of the system, thus it is most advantageous to fully focus on exploring the input space. In this study, the initial batch contained 100 samples.

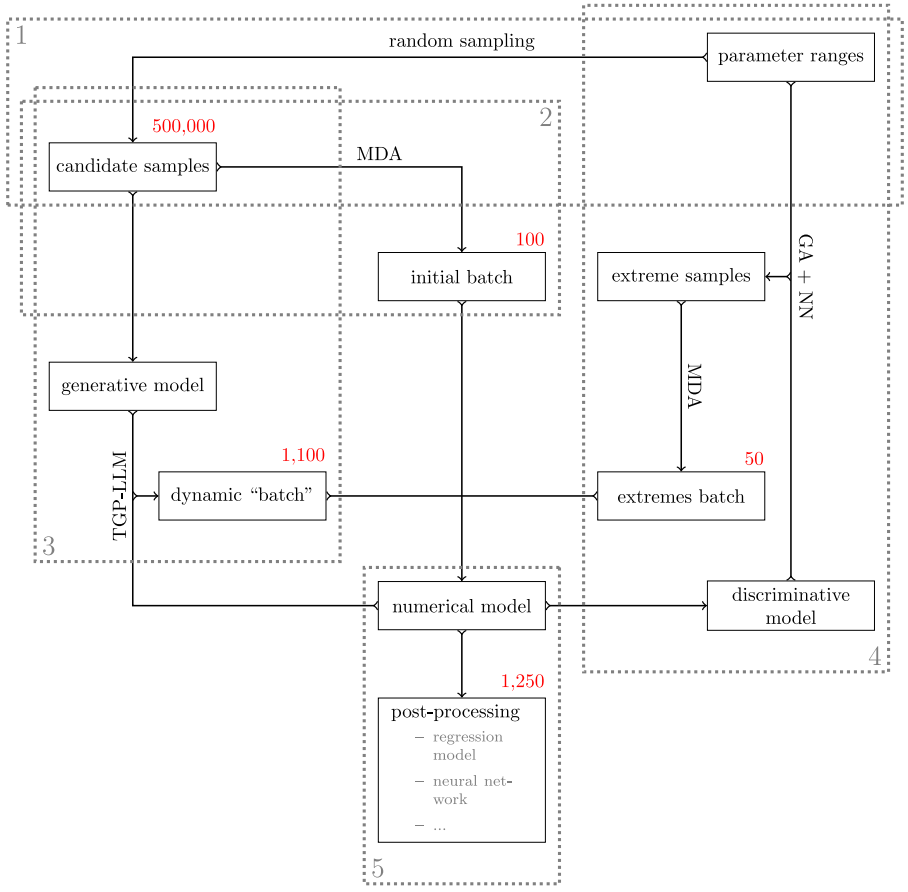

Fig. 1. Flowchart of the five-step simulation strategy. The numbers reflect the steps of the simulation strategy: (1) generate candidate samples, (2) simulate an initial batch, (3) execute an adaptive sampling approach, (4) simulate reverse-predicted extremes, and (5) post-process the data. The red-coloured values indicate the sample sizes of the data sets. MDA: Maximum Dissimilarity Algorithm; TGP-LLM: Treed Gaussian Process, Limiting Linear Model; GA: Genetic Algorithm; NN: neural network.

2.3. Adaptive sampling

The third step is most dissimilar from commonly employed sampling techniques, as in this step we used a generative model so that the selection of samples in the input space is based on the underlying distribution of the output space. In this study, the adaptive sampling was initiated by fitting a Treed Gaussian Process, Limiting Linear Model (TGP-LLM; Gramacy and Lee, 2009) to the incomplete output space resulting from the initial batch. The TGP-LLM determined the uncertainty in the output space and suggested which samples were most likely to reduce this uncertainty (Gramacy and Lee, 2009); here, uncertainty is defined by either the greatest standard deviation (active learning-MacKay; MacKay, 1992), or by the maximum expected reduction in the averaged squared error (active learning-Cohn; Cohn, 1996). As simulating regions with high uncertainty provide the highest entropy, these regions are most interesting to investigate further. This study made use of the active learning-MacKay approach: i.e. uncertainty was defined by the largest standard deviation.

The TGP-LLM method (Gramacy and Lee, 2009) was devised to optimally select candidate samples for asynchronous calculations on a supercomputer. The core of this generative method consists of fitting Gaussian process models to the input–output relations obtained from the available runs at a particular moment in the simulation procedure. These models are continuously updated as more results come in. In order to account for heteroscedasticity as well as non-linear behaviour of the output space in different subdomains of the input space, the Gaussian process model is combined with a Bayesian tree regression. This subdivides the input space in several subdomains that show different behaviour. Based on this statistical model, new candidate samples are chosen in order to fulfil different criteria. Most emphasis is placed on areas on the input space where the input–output variance is largest, so as to lead to an optimal reduction of the variance (maximum entropy approach). However, as this selection criterion may lead to exaggerated concentration of samples in a few places only, in addition care is taken to spread the candidate samples sufficiently over the different subdomains of the input space identified by the Bayesian tree regression, as well as to the sufficient spreading of candidate samples within these subdomains, in order to conserve the exploratory nature of the algorithm. For technical details on the method, we refer to Gramacy and Lee (2009).

Only a limited number of samples was selected by the TGP-LLM based on the initial batch. Subsequently, every time a simulation was finished, the TGP-LLM was re-fitted to the updated output space to determine the next input sample(s) with the highest entropy. This continued until a predefined number of samples was simulated. In this study, 1100 samples were generated and simulated using this adaptive approach.

2.4. Reverse-predict extremes

The fourth step is to search for extremes in the output space. This search was facilitated by means of a genetic algorithm (GA) for which the search for the extremes is an optimisation problem.

In order to obtain a fast tool to explore these extremes, a neural network was fitted to the available results from the MDA- and TGP-LLM-based samples. This neural network contained three hidden layers with 50 nodes each.

The implemented GA was designed such that a pool was created instead of the usual singular output. This pool consisted of output

values close to the most extreme—or optimal—value. Subsequently, a set of samples was drawn from this pool by using the MDA on the pool's unique samples. These samples were subsequently simulated to better represent the extremes in the data set.

2.5. Post-processing

The last step of post-processing the data is not as straightforward due to the absence of clear planes through the output space that can be assessed. Moreover, the commonly used methods for sensitivity analyses—such as Sobol' indices (Sobol, 1993, 2001) and ANOVA (Wang et al., 2020)—cannot be used due to the limited sample size.

Therefore, discriminative models have to be used over generative models that require larger data sets (Jebara, 2004). In this study we considered a neural network with the same architecture as described in Section 2.4 but which was retrained to the full data set, i.e., including the GA-based samples. More details on the neural network and its training are given in the *Supplementary Information* (Sec. *SI*-5).

3. Case study

This case study addresses the first step of developing nature-based solutions to mitigate salt intrusion. Thereby following the *Building with Nature*-approach, which is an approach to solve hydraulic engineering-related problems from a system-level point of view by utilising the system's natural processes (de Vriend et al., 2015). For that reason, the notion of *Building with Nature* has gained momentum in recent years. In the so-called nature-based solutions, the system is viewed from three perspectives: (1) physics, (2) ecology, and (3) socio-economy (van Slobbe et al., 2013). This multiperspective approach results in a very demanding design process.

A challenging phase in the *Building with Nature*-design procedure is to properly understand the underlying physical processes of a natural system, and how the engineering solution will utilise those to achieve certain socio-economic and ecological benefits. This principle is at the basis of the design procedure, and thus an essential feature (e.g. Borsje et al., 2011; van Slobbe et al., 2013; de Vriend et al., 2015).

3.1. Physical estuarine system

The methodology described in Section 2 is applied to a highly non-linear and non-stationary system to perform a sensitivity analysis: the estuary. Estuaries are complex systems largely due to the interaction of saline seawater and fresh river water. The induced density differences—albeit small—result in complex behaviour of the hydrodynamics, influencing flow structures, sediment dynamics, ecological functioning, and many other aspects (e.g. Geyer and MacCready, 2014; Olabarrieta et al., 2018; Whitfield et al., 2012; Zhou et al., 2020).

In this case study, the focus point is the salt intrusion length in an estuary and how this is influenced by the forcing and the estuarine geomorphology. The influence of the river discharge and water depth on the salt intrusion are well-known (e.g. Chatwin, 1976; Hansen and Rattray, 1965; MacCready, 2007; Monismith et al., 2002): negative and positive, respectively. Furthermore, the tide enhances the mixing of the water column and thereby influences the salt intrusion (e.g. MacCready and Geyer, 2010; Simpson et al., 1990). Other geomorphological features have also been investigated separately, such as the bottom curvature (Nunes and Simpson, 1985), tidal flats (Zhang et al., 2012), and meandering (Pein et al., 2018). All in all, many factors influence the salt intrusion length, generally in a non-linear fashion, and Table 1 summarises the input space used in this study.

Furthermore, estuaries behave differently based on their class—or type. Such classifications are often linked to the stratification of the system, and how this changes over a tidal cycle, as this largely determines the governing processes in an estuary (e.g. Dijkstra and Schuttelaars, 2021). The mapping of estuaries by Geyer and MacCready (2014) considers two non-dimensional variables in defining such a mapping, which is used in this study as indication of the distribution over the input space.

Table 1
Input parameters including their ranges and units; based on Dronkers (2017), Leuven et al. (2019), Savenije et al. (2008). Fig. 2 provides visual support of the input parameters. More information about the definitions of the input parameters and the physical restrictions are provided in the *Supplementary Information* (Secs. *SI*-1 and *SI*-2).

	Parameter	Symbol	Range	Unit
Forcing	Tidal range	a	1.0–5.0	m
	Storm surge level	η_s	0.0–2.0	m
	River discharge	Q	100–16,000	$m^3\ s^{-1}$
Geomorphology	Channel depth	d_c	5.0–25.0	m
	Channel width	W_c	500–3,000	m
	Channel friction	n_c	0.01–0.05	$m^{-1/3}s$
	Flat depth ratio[a]	r_d	−1–1	–
	Flat width	W_f	0–3,000	m
	Flat friction	n_f	0.02–0.05	$m^{-1/3}s$
	Convergence	γ	25–1.0	$\times 10^{-5}\ m^{-1}$
	Bottom curvature	κ_c	0.0–6.0	$\times 10^{-5}\ m^{-1}$
	Meander amplitude	A_m	0–6	km
	Meander length	L_m	0–100	km

[a]The flat depth is defined as the product of the flat depth ratio and the tidal range: $d_f = \frac{1}{2} r_d a$. Thereby ensuring that the tidal flats are at all times exposed and flooded during a tidal cycle, i.e. following the definition of a tidal flat.

The two non-dimensional variables are a mixing parameter (M, Eq. (1)) and the freshwater Froude number (Fr_f, Eq. (2)), which are indicative for the balancing forces in an estuary: mixing and stratification, respectively (Geyer and MacCready, 2014).

$$M = \sqrt{\frac{c_f u_t^2}{\omega_t N d_c^2}} \tag{1}$$

with

$$c_f = \frac{g n_c^2}{d_c^{1/3}}$$

$$u_t = \frac{1}{2\sqrt{2}} \sqrt{\frac{g}{d_c}} a$$

$$N = \sqrt{\frac{g \beta s_0}{d_c}}$$

where c_f is the non-dimensional friction coefficient [–]; u_t the tidal flow velocity [ms^{-1}]; ω_t the tidal frequency [s^{-1}]; N the buoyancy frequency [s^{-1}]; d_c the channel depth; and n_c the friction coefficient, defined as Manning's n [$m^{-1/3}s$]. In addition, there are three constants included: g is the gravitational acceleration [$g = 9.81\ ms^{-2}$]; β the haline contraction coefficient [$\beta = 7.6 \times 10^{-4}\ psu^{-1}$]; and s_0 the oceanic salinity [$s_0 = 30$ psu].

$$Fr_f = \frac{Q}{W_c d_c c_i} \tag{2}$$

with

$$c_i = \sqrt{d_c g \beta s_0}$$

where Q is the river discharge; W_c the channel width; and c_i the maximum frontal propagation speed, or internal celerity [ms^{-1}].

Note that not all parameters of the input space are included in this mapping (Table 1); this mapping does not address the occurrence of tidal flats or meandering of the estuary. Although it is not complete, the M, Fr_f-space by Geyer and MacCready (2014) provides good insights into the distribution of the data over the input space. For visual inspections, scatter plots of the distribution of input, output, and these non-dimensional parameters are included in the *Supplementary Information* (Fig. *SI*-2).

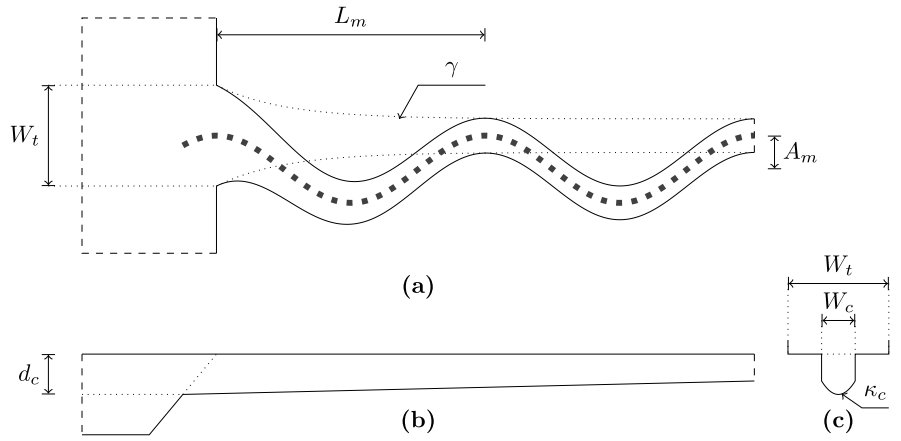

Fig. 2. Parametric model design zoomed-in near the estuary mouth. **(a)** Plan view; **(b)** longitudinal cross-section; and **(c)** lateral cross-section. The meaning of the symbols are presented in Table 1, except for W_t: This is the total width, i.e. $W_t = W_c + W_f$. The grey dots show the location of the "virtual stations" used for the output definitions (Eqs. (3a) and (3b)).

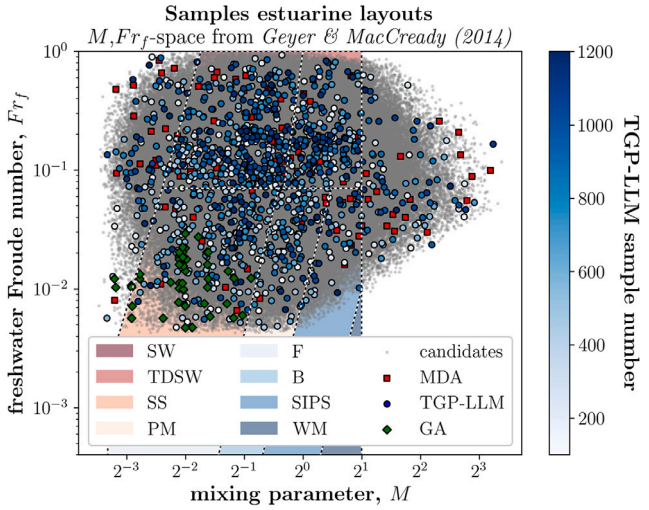

Fig. 3. Sample distributions with respect to the estuarine classification diagram by Geyer and MacCready (2014). SW: salt wedge; TDSW: time-dependent salt wedge; SS: strongly stratified; PM: partially mixed; F: fjord; B: bay; SIPS: strain-induced periodic stratification; WM: well-mixed; MDA: maximum dissimilarity algorithm; TGP-LLM: treed Gaussian process, limiting linear model; GA: genetic algorithm.

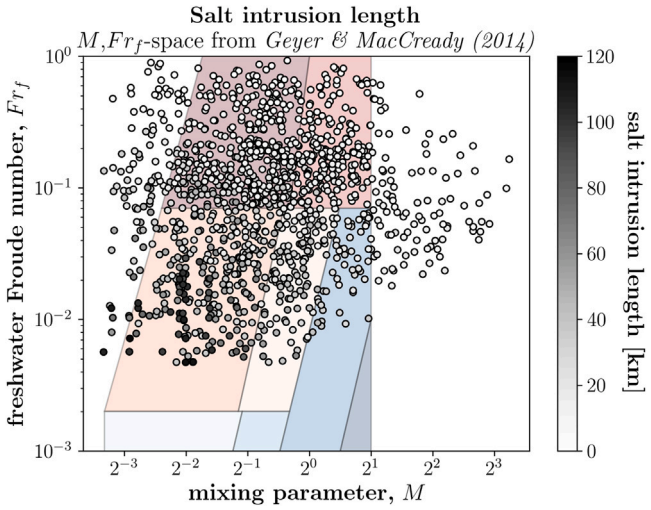

Fig. 4. Salt intrusion length with respect to the estuarine classification diagram by Geyer and MacCready (2014). Shading of estuarine classes as in Fig. 3.

3.2. Numerical experimental design

The simulations are performed using the Delft3D Flexible Mesh hydrodynamic modelling software (Deltares, 2022), where the model configurations are implemented by means of a parametric design. This software is a state-of-the-art process-based model that solves the Reynolds-averaged Navier–Stokes equations assuming hydrostatic pressure and using a $k-\varepsilon$ turbulence closure. Due to the focus on the salt dynamics, the simulations are carried out in three dimensions resulting in substantial computational costs.

The parametric design of the estuary follows an idealised geomorphology in which thirteen input parameters are reflected (Fig. 2): three forcing conditions and ten geomorphological features (see Table 1). These thirteen parameters are considered governing for the system investigated and are based on literature, as listed in Section 3.1 and Table 1. When a sparse factorial set of samples would have been used, almost 1.6 million ($N = 3^{13}$) simulations would have been required for the sensitivity analysis. In this study, approximately 1250 simulations were performed, where the sample size was in part based on economic considerations but extensively validated afterwards (see Section 5).

Because the case study encompasses a real physical system, there are some restrictions to parameter combinations, which result in dependencies between input parameters. Despite these dependencies, the restrictions are considered relaxed enough to provide enough space for every input parameter to move freely within its range. In essence, the restrictions function as a reduction of the input space required to explore. It does, however, also complicate the analyses by potential false cause-and-effect relations by showing a relation between an input parameter and the output space, while the real driving force is another input parameter. Therefore, one must remain cautious when analysing the data and keep the defined restrictions in mind.

More details on the parametric design, the physical restrictions, and the hydrodynamic model are presented in the *Supplementary Information* (Secs. *SI*-1, *SI*-2, and *SI*-4, resp.).

The output of the simulations is defined in two dimensions: (1) the salt intrusion length, $\mathcal{L}$; and (2) the salt variability, $\mathcal{V}$. These output variables are extracted from the model output data, which contains a longitudinal cross-section that follows the centre of the channel (dotted line in Fig. 2).

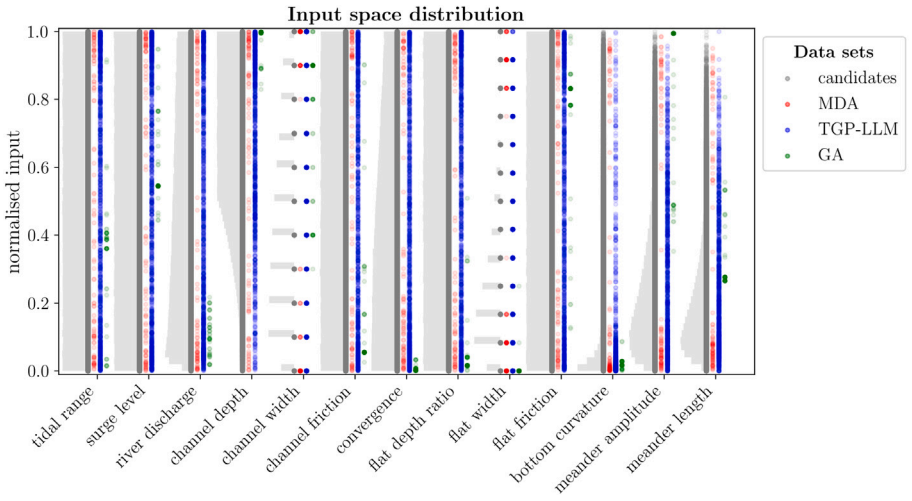

Fig. 5. Sampling distributions per input parameter and sampling method. The input parameters are normalised with a min–max scaling, where the ranges are as presented in Table 1.

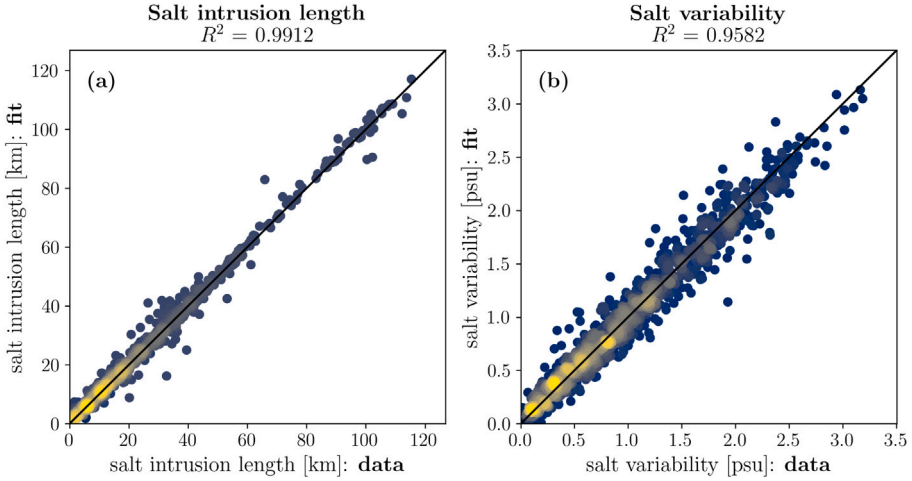

Fig. 6. Data fit of the neural network to both output variables: **(a)** salt intrusion length; and **(b)** salt variability. The colour-grading reflects the density of data points, where the dark blue reflects a low data density and the light yellow a high data density.

The salt intrusion length is defined as the distance from the mouth at which the depth-averaged salinity equals 1 psu, averaged over the tidal cycle. The salt variability is defined as the variation in salinity over a tidal cycle, i.e. the difference between the maximum and minimum salinity during a tidal cycle. This is taken as the average over the estuarine domain, using "virtual stations" every 625 metres (in x-direction). These definitions of the salt intrusion length ($\mathcal{L}$) and salt variability ($\mathcal{V}$) can be expressed as follows:

$$\mathcal{L} \equiv \overline{\delta\left(\langle s\rangle = 1\ [\text{psu}]\right)} \tag{3a}$$

$$\mathcal{V} \equiv \frac{1}{J}\sum_{j}^{J} \max_{T}\left\{\langle s\rangle_j\right\} - \min_{T}\left\{\langle s\rangle_j\right\} \tag{3b}$$

where δ is the distance from the mouth [m]; $\langle s\rangle$ the depth-averaged salinity [psu]; J the number of virtual stations in the model domain; and T the tidal period [s]. The overbar in Eq. (3a) represents tidal-averaging.

4. Results

The implementation of the proposed method is presented in three parts: (1) the distribution of samples for all three sampling methods employed (i.e. MDA, TGP-LLM, and GA; Section 4.1); (2) the skill of the trained neural network (Section 4.2); and (3) the progress of sampling in which the sample size of the adaptive sampling step is presented (Section 4.3), hinting towards potential stopping rules for this step. This order largely follows the work-flow introduced in Section 2 followed up by a reflection on the method.

Although the output space is defined by two variables (see Eqs. (3a) and (3b)), the main focus is on the salt intrusion length ($\mathcal{L}$, Eq. (3a)) due to its higher relevance and the correlation between the two output variables.

4.1. Sample distribution

All three sampling methods employed functioned as expected, even when considering their sampling selections in a different parameter space: Fig. 3 shows the candidate samples and the selected samples according to the different methods. Note that the GA did not make use of the candidate samples, as it generates samples as part of its algorithm; the MDA and TGP-LLM do create subsets from the candidate samples.

The MDA-based samples were clearly well-distributed throughout the whole two-dimensional parameter space and decently covered the outlines of the cloud of candidate samples. The undiscovered regions were subsequently well-covered by the samples from the TGP-LLM,

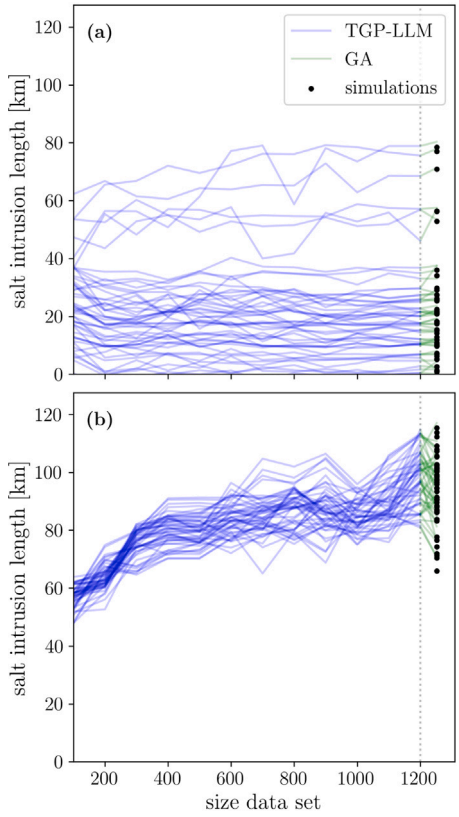

Fig. 7. Progress of predictive power of neural networks based on size of data set. **(a)** Randomly selected samples with average output values; and **(b)** samples with extreme output values, i.e. sampled with the genetic algorithm.

which had been able to select samples in the extremes of the parameter space as well; searching algorithms commonly tend to overlook the extremes. At last, the GA-based samples were specifically present in the *strongly stratified* estuary class, which also showed the largest salt intrusion length values (Fig. 4). As the GA was designed to search for the maxima in the salt intrusion length, this behaviour is as intended.

Supplementary to Fig. 3, Fig. 5 presents the distribution of the samples per input parameter—again, discriminating between the three implemented sampling methods. The three methods clearly show different distributions reflecting their underlying algorithms: (1) the MDA-based samples were clearly located at the extremes of the input space; (2) the TGP-LLM covered almost the whole input space with samples; and (3) the GA-based samples are located in the extremes of certain input parameters known to be of relevance for the salt intrusion length, such as the channel depth and the river discharge. As the GA was designed to search for extremes in the output space, this clustering of samples in the extremes of certain input parameters suggests a strong relation between these input parameters and the output. However, it is important to keep possible false cause-and-effect relations in mind when analysing the GA-based samples in Fig. 5.

4.2. Neural network performance

The neural network as introduced in Section 2.4 was trained to both output variables. The final neural network—as part of the last step (Section 2.5)—resulted in a great fit: salt intrusion length has $R^2_{\mathcal{L}} = 0.9912$; and for salt variability $R^2_{\mathcal{V}} = 0.9582$ (Fig. 6).

The neural network was trained—both in steps 4 and 5 of the method (Sections 2.4 and 2.5)—by splitting the available data in a training data set (80%) and a testing, or validation, data set (20%). The neural network only used the training data set to train during which the testing data set was never shown. Subsequently, the testing data set was used to determine the performance of the neural network; this was done to prevent over-fitting of the neural network to the data. More information on the training of the neural network can be found in the *Supplementary Information* (Sec. *SI*-5).

4.3. Sample size

As the data set grew, more data became available to train the neural network, hence the neural network improved its capabilities to represent the underlying relations. However, the extent of adaptive sampling to reach a satisfactory data set remained an open end.

To analyse the progress of system understanding as the data set grows, neural networks were trained at intervals of 100 samples. Note that the initial batch that contained 100 samples was drawn using only the MDA and was the starting point of the adaptive sampling. The intermediate neural networks were used to predict two types of samples: (1) randomly selected from the first 1202 samples, i.e. excluding the GA-based samples; and (2) the GA-based samples, reflecting the (expected) extremes in the output space.

As shown in Fig. 7a, recording the progress of the intermediate neural networks by means of a random selection is not informative: the neural network trained with 100 samples (i.e. MDA only) was already capable of predicting the simulated outputs quite well (black dots in Fig. 7a).

However, when looking at extreme values (Fig. 7b), a neural network trained on a larger data set showed substantial better predictive power, where the predictions seem to converge after a data set of around 800 samples. Although the predictions were not fully in line with the ground truth (black dots in Fig. 7b), a larger data set was better capable of indicating that there are extreme output values, while unable to predict the variance present in the extreme output space. The addition of the GA-based samples to the data set resulted in a substantial improvement, which is to be expected as these samples are representative for extremes in the output space. This improvement in predictive power of the neural network due to the GA-based samples is presented by the green lines in Fig. 7b—right of the grey, dotted line.

5. Discussion

This study aimed at gaining as much information about a complex system against the lowest computational costs. The resulting methodology provides a good understanding of such a complex system, namely salt intrusion in an estuary, while keeping the computational costs manageable.

For the comparison of computational efficiency, the minimum number of samples as stated by Wang et al. (2020) is used because the sample size is clearly defined. Sample sizes for, e.g., eFAST (Saltelli, 2002) or Sobol indices (Sobol, 1993) largely depend on the number of samples used for the Monte Carlo simulations—which are part of these methods. This introduces subjectivity to the chosen sample size, which makes them less suitable for such a comparison.

According to Wang et al. (2020), the number of samples for the sensitivity analysis with thirteen input parameters equals $N \geq 3^{13} = 1,594,323$, representing a sparse factorial input space. In contrast, the sample size used in this study equals only $N = 1,252$, which is a tremendous reduction in simulations, hence computational costs; more precisely, it is just shy of 0.08% of the samples in the factorial approach. Even though the application of the TGP-LLM creates computational overhead, this does not outweigh the removal of computational costs by reducing the sample size; the most efficient computational costs reduction remains shrinking the sample size. Furthermore, the implementation of the MDA and GA add a negligible computational overhead to the total costs.

Although the MDA is substantially cheaper than the TGP-LLM and is able to explore the input space well, it has a smaller coverage of the output space (Figs. 8b and c). It does, however, cover more of the output space compared to, e.g., random sampling (Fig. 8a).

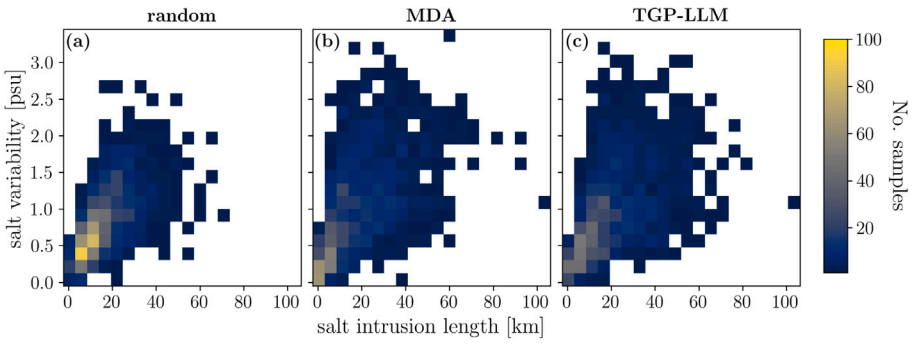

Fig. 8. The coverage of the two-dimensional output space for three sampling methods: **(a)** random sampling, **(b)** MDA, and **(c)** TGP-LLM. Note that the data sets are of equal size and the samples derived with the GA are not included in **(c)** but the initial, MDA-based batch is. The output spaces are generated with the neural network for compatibility.

Furthermore, the MDA is a non-adaptive selection method—i.e. solely based on the input space—, while the TGP-LLM draws samples based on the output space. This principle has benefits on itself: The aim of the MDA is to explore the input space, while the TGP-LLM aims to "understand" the output space.

Despite almost completely diminishing the sample size compared to the aforementioned methods, the large coverage of the samples allows for a good system understanding (Fig. 3). This is further enhanced by using a neural network to augment the output space. This augmentation step is crucial as it greatly enhances the understanding of a complex system without the need for additional expensive numerical model simulations.

The relevance of simulating the extremes in the output space for the performance of the neural network becomes apparent from Fig. 7. However, it also raises the question whether to wait for so many (expensive) numerical model simulations to apply the genetic algorithm; especially when analysing Fig. 9. Fig. 9 shows a similar figure as Fig. 7 with the major difference being the addition of the GA-based samples to the data set before training the intermediate neural networks. The result is a tremendous improvement of all intermediate neural networks in their predictive power, also for extremes in the output space.

However, analysing solely Fig. 9 would result in the misleading conclusion that there was no need for more than 150 simulations, i.e. the MDA- and GA-based samples. In addition to the fact that a data fit improves with more data, training the neural network with a small data set shows substantial inconsistencies in its predictions, which is clearly shown in Fig. 10. The shading around the training error represents the spreading of the root-mean-squared-error during training, which is indicative for the inconsistency of the predictions; the predictions become more consistent with increasing size of the data sets used (Fig. 10).

Furthermore, the GA-based samples that cause such a performance boost in Fig. 9b are drawn using a neural network trained with 1202 samples. However, this information is not available during the adaptive sampling and, therefore, cannot be used.

Nevertheless, the genetic algorithm could have been employed at an earlier stage, resulting in a similar predictive power of the final neural network. This conclusion could also be drawn from looking at Fig. 3, where the last 100–200 samples seem to be concentrated in already densely populated areas in the input space; and from Fig. 7b, where the predictions of the intermediate neural networks seem to converge after approximately 800 samples.

Furthermore, the neural networks trained with smaller data sets are already able to detect the regions in the input space with extreme values in the output space. This is reflected by Fig. 11 in which the implementation of the GA with the intermediate trained neural networks all favour samples located at low values of the mixing parameter (M) and freshwater Froude number (Fr_f), which result in the largest salt intrusion length (Fig. 4).

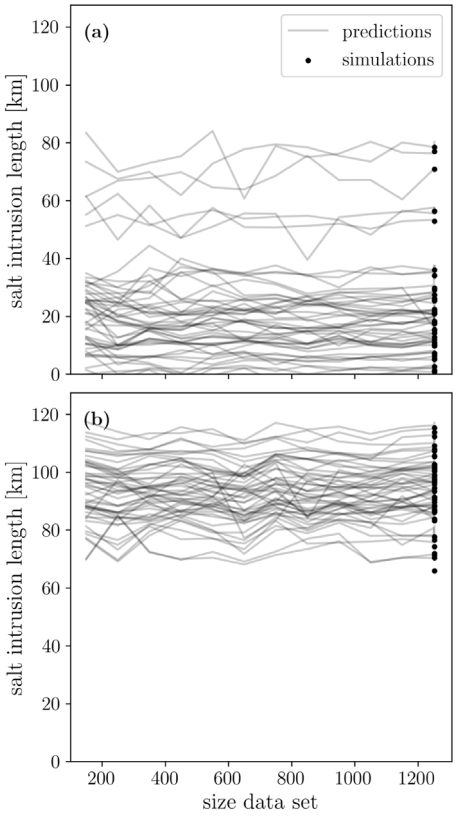

Fig. 9. Progress of predictive power of neural networks based on size of data set, where the samples derived with the genetic algorithm are included at every step. **(a)** Randomly selected samples with average output values; and **(b)** samples with extreme output values, i.e. sampled with the genetic algorithm.

However, the GA-pools generated with smaller data sets (1) show a wider spreading, which can be traced back to the inconsistent predictions presented in Fig. 10; and (2) include samples from regions with lower values of the salt intrusion length, as shown by Fig. 4. In addition, the estimates of salt intrusion length determined by the intermediately trained neural networks increases with increasing size of the data set used (Fig. 11).

6. Conclusion

The proposed simulation strategy mainly focuses on the first and last steps of HD—namely the sampling and the augmentation—while

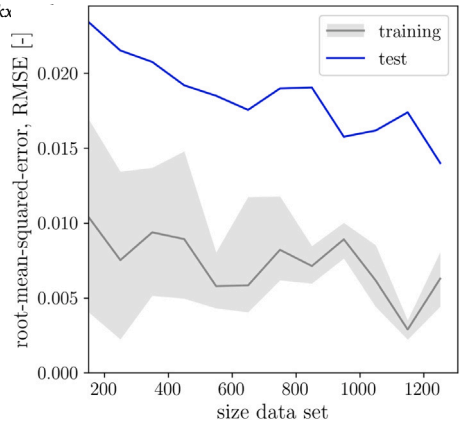

Fig. 10. Uncertainty in predictions of intermediate neural networks.

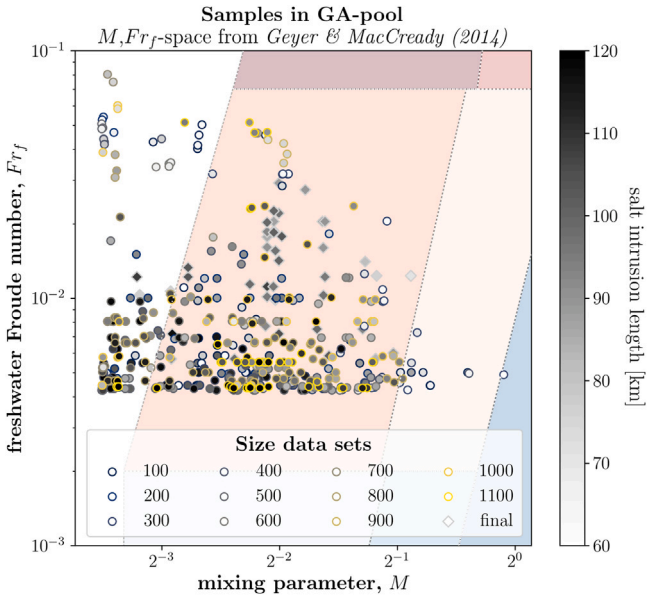

Fig. 11. Samples in the GA-pool determined with the intermediate trained neural networks overlayed on the estuarine classification diagram by Geyer and MacCready (2014). Shading of estuarine classes as in Fig. 3. The grey-shading reflects the salt intrusion length, and the edge-colour the size of the data sets.

implementing an expensive, process-based numerical model for the second step—the simulations. The strategy has achieved a major reduction in computational costs by making informed choices in the selection of samples to simulate. Subsequently, the augmentation is facilitated by means of a neural network, which shows to reliably predict the highly non-linear output space (Fig. 6).

In the case study addressed in this study, the extremes in the output space have a substantial effect on the level of system understanding achieved (Figs. 7 and 9). Therefore, the simulation strategy is expected to be improved by employing the genetic algorithm at an earlier stage, or on multiple occasions at certain intervals. However, a sufficiently large data set is required to reliably train a neural network—or fit another data-driven model—to be used in the objective function of the genetic algorithm, as illustrated by Fig. 10.

Reflecting on the aim of this study (Section 1), this paper has shown the potential of techniques from machine learning for hydraulic engineering practices, with a special focus on enabling the *Building with Nature*-approach. Sensitivity analyses are a useful method to gain insights into the system's behaviour, but generally require large amounts of samples—i.e. simulations. Due to the complexity of models in the field of hydraulic engineering, this often results in computationally infeasible studies: a challenge complicating the evaluation of adaptation and mitigation strategies. This study has shown that hybrid downscaling with techniques from machine learning enables the execution of enlightening sensitivity analyses to come within computational reach. The approach facilitates exploratory studies essential for the development of future-proof socio-ecological systems, especially in light of unknown system states resulting from climate change.

Software availability

The trained and implemented neural network is open-access, named ANNESI (Artificial Neural Network for Estuarine Salt Intrusion; Hendrickx, 2022).

CRediT authorship contribution statement

Gijs G. Hendrickx: Designed the research, Performed the research, Analysed the data, Wrote the manuscript, Reviewed the manuscript. **José A.A. Antolínez:** Designed the research, Analysed the data, Reviewed the manuscript. **Peter M.J. Herman:** Designed the research, Analysed the data, Reviewed the manuscript.

Declaration of competing interest

The authors declare that they have no known competing financial interests or personal relationships that could have appeared to influence the work reported in this paper.

Data availability

The dataset used in this study is publicly available as NEESI: Numerical Experiments of Estuarine Salt Intrusion dataset (Hendrickx, 2023).

Acknowledgements

We are indebted to Ariana Torres (SURF) for her support in the development of the computational manager for the many simulations executed. This work used the Dutch national e-infrastructure with the support of the SURF Cooperative using grant no. EINF-1548. At last, we would like to thank the two anonymous reviewers for their valuable feedback on the manuscript.

Funding

This publication is part of the project "Design and operation of nature-based SALTISolutions" (with project number P18-32 Project 7) of the research programme SALTISolutions which is (partly) financed by the Dutch Research Council (NWO).

Appendix A. Supplementary data

Supplementary material related to this article can be found online at https://doi.org/10.1016/j.coastaleng.2023.104289.

References

Anderson, D., Ruggiero, P., Antolínez, J.A.A., Méndez, F.J., Allan, J., 2018. A climate index optimized for longshore sediment transport reveals interannual and multidecadal littoral cell rotations. J. Geophys. Res.: Earth Surf. 123 (8), 1958–1981. http://dx.doi.org/10.1029/2018JF004689.

Antolínez, J.A.A., Méndez, F.J., Anderson, D., Ruggiero, P., Kaminsky, G.M., 2019. Predicting climate-Driven Coastlines with a simple and efficient multiscale model. J. Geophys. Res.: Earth Surf. 124 (6), 1596–1624. http://dx.doi.org/10.1029/2018JF004790.

Antolínez, J.A.A., Méndez, F.J., Camus, P., Vitousek, S., Gonzales, E.M., Ruggiero, P., Barnard, P., 2016. A multiscale climate emulator for long-term morphodynamics (MUSCLE-morpho). J. Geophys. Res.: Oceans 121, 775–791. http://dx.doi.org/10.1002/2015JC011107.

Antolínez, J.A.A., Murray, A.B., Méndez, F.J., Moore, L.J., Farley, G., Wood, J., 2018. Downscaling changing coastlines in a changing climate: The hybrid approach. J. Geophys. Res.: Earth Surf. 123 (2), 229–251. http://dx.doi.org/10.1002/2017JF004367.

Ashton, A., Murray, A.B., Arnault, O., 2001. Formation of coastline features by large-scale instabilities induced by high-angle waves. Nature 414 (6861), 296–300. http://dx.doi.org/10.1038/35104541, https://www.nature.com/articles/35104541.

Athanasiou, P., van Dongeren, A., Giardino, A., Vousdoukas, M., Antolínez, J.A.A., Ranasinghe, R., 2021. A clustering approach for predicting dune morphodynamic response to storms using typological coastal profiles: A case study at the Dutch coast. Front. Marine Sci. 8 (September), 1–20. http://dx.doi.org/10.3389/fmars.2021.747754.

Athanasiou, P., van Dongeren, A., Giardino, A., Vousdoukas, M., Antolínez, J.A.A., Ranasinghe, R., 2022. Estimating dune erosion at the regional scale using a meta-model based on neural networks. Nat. Hazard. Earth Syst. Sci. Dis. 22, 3897–3915.

Bakker, T.M., Antolínez, J.A.A., Leijnse, T.W.B., Pearson, S.G., Giardino, A., 2022. Estimating tropical cyclone-induced wind, waves, and surge: A general methodology based on representative tracks. Coast. Eng. 176, 104154. http://dx.doi.org/10.1016/j.coastaleng.2022.104154.

van Berchum, E.C., Mobley, W., Jonkman, S.N., Timmermans, J.S., Kwakkel, J.H., Brody, S.D., 2019. Evaluation of flood risk reduction strategies through combinations of interventions. J. Flood Risk Manag. 12, e12506. http://dx.doi.org/10.1111/jfr3.12506.

Borsje, B.W., van Wesenbeeck, B.K., Dekker, F., Paalvast, P., Bouma, T.J., van Katwijk, M.M., de Vries, M.B., 2011. How ecological engineering can serve in coastal protection. Ecol. Eng. 37 (2), 113–122. http://dx.doi.org/10.1016/j.ecoleng.2010.11.027, https://linkinghub.elsevier.com/retrieve/pii/S0925857410003216.

Bruun, P., 1954. Coast erosion and the development of beach profiles. In: Beach Erosion Board Technical Memorandum. No. 44. Tech. Rep., US Army Corps of Engineers, Vicksburg, MS, USA, p. 79.

Camus, P., Mendez, F.J., Medina, R., Cofiño, A.S., 2011. Analysis of clustering and selection algorithms for the study of multivariate wave climate. Coast. Eng. 58 (6), 453–462. http://dx.doi.org/10.1016/j.coastaleng.2011.02.003.

Chatwin, P.C., 1976. Some remarks on the maintenance of the salinity distribution in estuaries. Estuar. Coast. Mar. Sci. 4 (5), 555–566. http://dx.doi.org/10.1016/0302-3524(76)90030-X.

Chen, C., Beardsley, R.C., Cowles, G., Qi, J., Lai, Z., Gao, G., Stuebe, D., Liu, H., Xu, Q., Xue, P., Ge, J., Hu, S., Ji, R., Tian, R., Huang, H., Wu, L., Lin, H., Sun, Y., Zhao, L., 2013. An Unstructured Grid, Finite-Volume Community Ocean Model FVCOM User Manual. Tech. Rep., University of Massachusetts-Dartmouth, New Bedford, MA, USA, p. 404.

Cohn, D.A., 1996. Neural network exploration using optimal experiment design. Neural Netw. 9 (6), 1071–1083. http://dx.doi.org/10.1016/0893-6080(95)00137-9.

Collins, L., Bradstock, R.A., Clarke, H., Clarke, M.F., Nolan, R.H., Penman, T.D., 2021. The 2019/2020 mega-fires exposed Australian ecosystems to an unprecedented extent of high-severity fire. Environ. Res. Lett. 16 (4), 044029. http://dx.doi.org/10.1088/1748-9326/abeb9e.

Deltares, 2022. Delft3D Flexible Mesh, User Manual. Delft, the Netherlands, p. 449.

Dijkstra, Y.M., Schuttelaars, H.M., 2021. A unifying approach to subtidal salt intrusion modeling in tidal estuaries. J. Phys. Oceanogr. 51 (1), 147–167. http://dx.doi.org/10.1175/jpo-d-20-0006.1.

Dronkers, J., 2017. Convergence of estuarine channels. Cont. Shelf Res. 144, 120–133. http://dx.doi.org/10.1016/j.csr.2017.06.012.

Geyer, W.R., MacCready, P., 2014. The estuarine circulation. Annu. Rev. Fluid Mech. 46 (1), 175–197. http://dx.doi.org/10.1146/annurev-fluid-010313-141302, https://www.annualreviews.org/doi/10.1146/annurev-fluid-010313-141302.

Gramacy, R.B., Lee, H.K., 2009. Adaptive design and analysis of supercomputer experiments. Technometrics 51 (2), 130–145. http://dx.doi.org/10.1198/TECH.2009.0015.

Haasnoot, M., van Deursen, W.P., Guillaume, J.H., Kwakkel, J.H., van Beek, E., Middelkoop, H., 2014. Fit for purpose? Building and evaluating a fast, integrated model for exploring water policy pathways. Environ. Model. Softw. 60, 99–120. http://dx.doi.org/10.1016/j.envsoft.2014.05.020.

Hansen, D.V., Rattray, M., 1965. Gravitational circulation in straits and estuaries. J. Mar. Res. 23, 104–122.

Harley, C.D.G., Hughes, A.R., Hultgren, K.M., Miner, B.G., Sorte, C.J.B., Thornber, C.S., Rodriguez, L.F., Tomanek, L., Williams, S.L., 2006. The impacts of climate change in coastal marine systems. Ecol. Lett. 9 (2), 228–241. http://dx.doi.org/10.1111/j.1461-0248.2005.00871.x.

Hendrickx, G.G., 2022. ANNESI: An open-source artificial neural network for estuarine salt intrusion. 4TU.ResearchData, http://dx.doi.org/10.4121/19307693.

Hendrickx, G.G., 2023. NEESI: Numerical Experiments of Estuarine Salt Intrusion dataset. 4TU.ResearchData, http://dx.doi.org/10.4121/22272247.

Hendrickx, G.G., Herman, P.M.J., Dijkstra, J.T., Storlazzi, C.D., Toth, L.T., 2021. Online-coupling of widely-ranged timescales to model coral reef development. Environ. Model. Softw. 143, 105103. http://dx.doi.org/10.1016/j.envsoft.2021.105103, https://linkinghub.elsevier.com/retrieve/pii/S1364815221001468.

Hughes, T.P., Anderson, K.D., Connolly, S.R., Heron, S.F., Kerry, J.T., Lough, J.M., Baird, A.H., Baum, J.K., Berumen, M.L., Bridge, T.C.L., Claar, D.C., Eakin, C.M., Gilmour, J.P., Graham, N.A., Harrison, H., Hobbs, J.P.A., Hoey, A.S., Hoogenboom, M., Lowe, R.J., McCulloch, M.T., Pandolfi, J.M., Pratchett, M., Schoepf, V., Torda, G., Wilson, S.K., 2018. Spatial and temporal patterns of mass bleaching of corals in the Anthropocene. Science 359 (6371), 80–83. http://dx.doi.org/10.1126/science.aan8048.

Itzkin, M., Moore, L.J., Ruggiero, P., Hovenga, P.A., Hacker, S.D., 2022. Combining process-based and data-driven approaches to forecast beach and dune change. Environ. Model. Softw. 153, 105404. http://dx.doi.org/10.1016/j.envsoft.2022.105404.

Jebara, T., 2004. Machine Learning: Discriminative and Generative, first ed. Springer Science+Business Media New York, p. 197. http://dx.doi.org/10.1007/978-1-4419-9011-2.

Kennard, R.W., Stone, L.A., 1969. Computer aided design of experiments. Technometrics 11 (1), 137–148. http://dx.doi.org/10.1080/00401706.1969.10490666.

Kohonen, T., 1982. Self-organized formation of topologically correct feature maps. Biol. Cybernet. 43 (1), 59–69. http://dx.doi.org/10.1007/BF00337288.

Kragtwijk, N.G., Zitman, T.J., Stive, M.J., Wang, Z.B., 2004. Morphological response of tidal basins to human interventions. Coast. Eng. 51 (3), 207–221. http://dx.doi.org/10.1016/j.coastaleng.2003.12.008.

Kuijper, K., van Rijn, L.C., 2011. Analytical and numerical analysis of tides and salinities in estuaries; Part II: Salinity distributions in prismatic and convergent tidal channels. Ocean Dyn. 61 (11), 1743–1765. http://dx.doi.org/10.1007/s10236-011-0454-z, https://link.springer.com/article/10.1007/s10236-011-0454-z.

Latteux, B., 1995. Techniques for long-term morphological simulation under tidal action. Mar. Geol. 126 (1–4), 129–141. http://dx.doi.org/10.1016/0025-3227(95)00069-B.

Leuven, J.R.F.W., Pierik, H.J., van der Vegt, M., Bouma, T.J., Kleinhans, M.G., 2019. Sea-level-rise-induced threats depend on the size of tide-influenced estuaries worldwide. Nature Clim. Change 9 (12), 986–992. http://dx.doi.org/10.1038/s41558-019-0608-4.

Luijendijk, A.P., de Schipper, M.A., Ranasinghe, R., 2019. Morphodynamic acceleration techniques for multi-timescale predictions of complex sandy interventions. J. Mar. Sci. Eng. 7 (3), 78. http://dx.doi.org/10.3390/jmse7030078, https://www.mdpi.com/2077-1312/7/3/78.

MacCready, P., 1999. Estuarine adjustment to changes in river flow and tidal mixing. J. Phys. Oceanogr. 29 (4), 708–726. http://dx.doi.org/10.1175/1520-0485(1999)029<0708:EATCIR>2.0.CO;2.

MacCready, P., 2007. Estuarine adjustment. J. Phys. Oceanogr. 37 (8), 2133–2145. http://dx.doi.org/10.1175/JPO3082.1, http://journals.ametsoc.org/jpo/article-pdf/37/8/2133/4487483/jpo3082_1.pdf.

MacCready, P., Geyer, W.R., 2010. Advances in estuarine physics. Ann. Rev. Mar. Sci. 2 (1), 35–58. http://dx.doi.org/10.1146/annurev-marine-120308-081015, http://www.annualreviews.org/doi/10.1146/annurev-marine-120308-081015.

MacKay, D.J.C., 1992. Information-based objective functions for active data selection. Neural Comput. 4 (4), 590–604. http://dx.doi.org/10.1162/neco.1992.4.4.590.

McKay, M.D., Beckman, R.J., Conover, W.J., 1979. A comparison of three methods for selecting values of input variables in the analysis of output from a computer code. Technometrics 21 (2), 239–245. http://dx.doi.org/10.1080/00401706.2000.10485979.

Monismith, S.G., Kimmerer, W., Burau, J.R., Stacey, M.T., 2002. Structure and flow-induced variability of the subtidal salinity field in northern San Francisco Bay. J. Phys. Oceanogr. 32 (11), 3003–3019. http://dx.doi.org/10.1175/1520-0485(2002)032<3003:SAFIVO>2.0.CO;2.

Nunes, R.A., Simpson, J.H., 1985. Axial convergence in a well-mixed estuary. Estuar. Coast. Shelf Sci. 20 (5), 637–649. http://dx.doi.org/10.1016/0272-7714(85)90112-X.

Olabarrieta, M., Geyer, W.R., Coco, G., Friedrichs, C.T., Cao, Z., 2018. Effects of density-driven flows on the long-term morphodynamic evolution of funnel-shaped estuaries. J. Geophys. Res.: Earth Surf. 123 (11), 2901–2924. http://dx.doi.org/10.1029/2017JF004527, https://agupubs.onlinelibrary.wiley.com/doi/10.1029/2017JF004527.

Pein, J., Valle-Levinson, A., Stanev, E.V., 2018. Secondary circulation asymmetry in a meandering, partially stratified estuary. J. Geophys. Res.: Oceans 123 (3), 1670–1683. http://dx.doi.org/10.1002/2016JC012623.

Ralston, D.K., Geyer, W.R., Lerczak, J.A., 2010. Structure, variability, and salt flux in a strongly forced salt wedge estuary. J. Geophys. Res.: Oceans 115 (6), http://dx.doi.org/10.1029/2009JC005806.

Rueda, A., Cagigal, L., Pearson, S., Antolínez, J.A.A., Storlazzi, C.D., van Dongeren, A., Camus, P., Mendez, F.J., 2019. HyCReWW: A Hybrid Coral Reef Wave and Water level metamodel. Comput. Geosci. 127, 85–90. http://dx.doi.org/10.1016/j.cageo.2019.03.004.

Ruessink, B.G., 2006. A Bayesian estimation of parameter-induced uncertainty in a nearshore alongshore current model. J. Hydroinform. 8 (1), 37–49. http://dx.doi.org/10.2166/jh.2006.009, http://iwaponline.com/jh/article-pdf/8/1/37/392771/37.pdf.

Saltelli, A., 2002. Making best use of model evaluations to compute sensitivity indices. Comput. Phys. Comm. 145 (2), 280–297. http://dx.doi.org/10.1016/S0010-4655(02)00280-1.

Saltelli, A., Tarantola, S., Chan, K.P., 1999. A quantitative model-independent method for global sensitivity analysis of model output. Technometrics 41 (1), 39–56. http://dx.doi.org/10.1080/00401706.1999.10485594.

Savenije, H.H.G., Toffolon, M., Haas, J., Veling, E.J.M., 2008. Analytical description of tidal dynamics in convergent estuaries. J. Geophys. Res.: Oceans 113 (10), http://dx.doi.org/10.1029/2007JC004408, https://agupubs.onlinelibrary.wiley.com/doi/10.1029/2007JC004408.

Scott, F., Antolínez, J.A.A., McCall, R., Storlazzi, C., Reniers, A., Pearson, S., 2020. Hydro-morphological characterization of coral reefs for wave runup prediction. Front. Mar. Sci. 7, 361. http://dx.doi.org/10.3389/fmars.2020.00361.

Simpson, J.H., Brown, J., Matthews, J., Allen, G., 1990. Tidal straining, density currents, and stirring in the control of estuarine stratification. Estuaries 13 (2), 125–132. http://dx.doi.org/10.2307/1351581, https://link.springer.com/article/10.2307/1351581.

van Slobbe, E., de Vriend, H.J., Aarninkhof, S.G.J., Lulofs, K., de Vries, M., Dircke, P., 2013. Building with Nature: In search of resilient storm surge protection strategies. Nat. Hazards 65 (1), 947–966. http://dx.doi.org/10.1007/s11069-012-0342-y, https://link.springer.com/article/10.1007/s11069-012-0342-y.

Sobol, I.M., 1993. Sensitivity estimates for nonlinear mathematical models. Math. Model. Comput. Exper. 1 (4), 407–414.

Sobol, I.M., 2001. Global sensitivity indices for nonlinear mathematical models and their Monte Carlo estimates. Math. Comput. Simulation 55 (1–3), 271–280. http://dx.doi.org/10.1016/S0378-4754(00)00270-6.

Stockdon, H.F., Holman, R.A., Howd, P.A., Sallenger, A.H., 2006. Empirical parameterization of setup, swash, and runup. Coast. Eng. 53 (7), 573–588. http://dx.doi.org/10.1016/j.coastaleng.2005.12.005.

Toreti, A., Bavera, D., Acosta Navarro, J., Cammalleri, C., de Jager, A., Di Ciollo, C., Hrast Essenfelder, A., Maetens, W., Masante, D., Magni, D., Mazzeschi, M., Spinoni, J., 2022. Drought in Europe August 2022. Tech. Rep., Publications Office of the European Union, Luxembourg, http://dx.doi.org/10.2760/264241.

Veldkamp, T.I., Wada, Y., de Moel, H., Kummu, M., Eisner, S., Aerts, J.C., Ward, P.J., 2015. Changing mechanism of global water scarcity events: Impacts of socioeconomic changes and inter-annual hydro-climatic variability. Global Environ. Change 32, 18–29. http://dx.doi.org/10.1016/j.gloenvcha.2015.02.011.

Vörösmarty, C.J., Green, P., Salisbury, J., Lammers, R.B., 2000. Global water resources: Vulnerability from climate change and population growth. Science 289 (5477), 284–288. http://dx.doi.org/10.1126/science.289.5477.284, https://www.science.org/doi/abs/10.1126/science.289.5477.284.

de Vriend, H.J., Capobianco, M., Chesher, T., de Swart, H.E., Latteux, B., Stive, M.J.F., 1993. Approaches to long-term modelling of coastal morphology: A review. Coast. Eng. 21 (1–3), 225–269. http://dx.doi.org/10.1016/0378-3839(93)90051-9.

de Vriend, H.J., van Koningsveld, M., Aarninkhof, S.G.J., de Vries, M.B., Baptist, M.J., 2015. Sustainable hydraulic engineering through Building with Nature. J. Hydro-Environ. Res. 9 (2), 159–171. http://dx.doi.org/10.1016/j.jher.2014.06.004, https://www.sciencedirect.com/science/article/pii/S1570644314000653.

Walstra, D.J.R., Hoekstra, R., Tonnon, P.K., Ruessink, B.G., 2013. Input reduction for long-term morphodynamic simulations in wave-dominated coastal settings. Coast. Eng. 77, 57–70. http://dx.doi.org/10.1016/j.coastaleng.2013.02.001.

Walther, G.R., Post, E., Convey, P., Menzel, A., Parmesan, C., Beebee, T.J., Fromentin, J.M., Hoegh-Guldberg, O., Bairlein, F., 2002. Ecological responses to recent climate change. Nature 416 (6879), 389–395. http://dx.doi.org/10.1038/416389a.

Wang, F., Huang, G.H., Fan, Y., Li, Y.P., 2020. Robust subsampling ANOVA methods for sensitivity analysis of water resource and environmental models. Water Res. Manag. 34 (10), 3199–3217. http://dx.doi.org/10.1007/s11269-020-02608-2.

Warner, J.C., Geyer, W.R., Lerczak, J.A., 2005. Numerical modeling of an estuary: A comprehensive skill assessment. J. Geophys. Res.: Oceans 110 (5), 1–13. http://dx.doi.org/10.1029/2004JC002691, https://agupubs.onlinelibrary.wiley.com/doi/10.1029/2004JC002691.

Whitfield, A.K., Elliott, M., Basset, A., Blaber, S.J.M., West, R.J., 2012. Paradigms in estuarine ecology - A review of the Remane diagram with a suggested revised model for estuaries. Estuar. Coast. Shelf Sci. 97, 78–90. http://dx.doi.org/10.1016/j.ecss.2011.11.026.

Zhang, Z., Cui, B., Fan, X., Zhang, K., Zhao, H., Zhang, H., 2012. Wetland network design for mitigation of saltwater intrusion by replenishing freshwater in an estuary. Clean - Soil Air Water 40 (10), 1036–1046. http://dx.doi.org/10.1002/clen.201100735.

Zhou, Z., Chen, L., Tao, J., Gong, Z., Guo, L., van der Wegen, M., Townend, I., Zhang, C., 2020. The role of salinity in fluvio-deltaic morphodynamics: A long-term modelling study. Earth Surf. Process. Landf. 45 (3), 590–604. http://dx.doi.org/10.1002/esp.4757.